Accepted manuscript doi:
10.1680/jstbu.21.00116

Submitted: 13 July 2021

Published online in 'accepted manuscript' format: 25 October 2023

Manuscript title: Numerical modelling of concrete-filled rectangular tubular flange girders subjected to pure bending

Authors: Rana Al-Dujele[1,2] and Katherine A. Cashell[3]

Affiliations: [1]Department of Civil Engineering, Uruk University, Baghdad, Iraq; [2]Department of Civil and Environmental Engineering, Brunel University London, Middlesex, UK and [3]Department of Civil, Environmental and Geomatic Engineering, University College London (UCL), London, UK

Corresponding author: Rana Al-Dujele, Department of Civil Engineering, Uruk University, Baghdad, Iraq.

E-mail: rana.aldujele@uruk.edu.iq

Accepted manuscript doi:
10.1680/jstbu.21.00116

Abstract

A detailed study of the behaviour of concrete filled rectangular tubular flange girders (CFRFGs) is described in this paper. These are steel beams in which the top flange plate is replaced with a concrete-filled steel section, resulting in greater load-carrying capacity and lateral torsional buckling resistance compared with a regular steel beam of similar proportions. These are complex members and their behaviour is governed by several inter-related parameters which are studied and discussed herein. Using the Abaqus program, a three-dimensional finite element model is developed to investigate the flexural behaviour of simply supported CFRFGs. Using available experimental results; the computational model is validated and is then employed to study the influence of the most salient properties on the overall response. A simplified analytical model is presented based on a fundamental assessment of the behaviour, to predict the capacity of these types of section in a way that is suitable for designers. The results are compared to those from the finite element analysis and it is shown that the analytical model is capable of providing an accurate depiction of the behaviour and the capacity of bending moment.

Keywords: Finite element analysis; composite construction; concrete-filled tubes; concrete confinement; heavily loaded structures; efficient design

Accepted manuscript doi:
10.1680/jstbu.21.00116

1. Introduction

Composite construction is increasingly popular in structural design, owing to the efficient use of the constituent materials and the ready availability of good design methods for standard members. The research community has contributed hugely to this surge in popularity by developing a fundamental understanding of the structural behaviour, conducting detailed analysis and proposing useful design approaches both for individual components as well as composite structural systems. In recent years, the behaviour of concrete-filled steel tubes (CFST) has been attracting considerable attention from the research and design community. These have beneficial qualities in terms of strength, stiffness and constructability (Ge and Usami 1992). The concrete core not only adds to the strength of the member but may also prevent local buckling of the steel tube and increase the overall stability of the member as a system. On the other hand, the steel tube provides confining pressure to the concrete, forcing it in to a triaxial compressive stress state (Mollazadeh 2015).

The focus of the current paper is on a relatively new section type which is quite similar to the CFST, called a concrete filled rectangular flange girder (CFRFG). These are created by replacing the top flange plate of a conventional universal beam with a concrete filled steel tube. A number of different types of composite cross-section comprising concrete filled and hollow tubular flanges have been developed for buildings and bridges, mainly for heavily loaded applications which could not be supported by standard rolled sections or plate girders (Chung and Lawson 2001). They have been employed in bridge applications, such as in Lynch Village in the US, which was constructed in 2010 and is one of the earliest examples of a concrete filled tubular flange girder (CFTFG) being used in bridges.

In the US, researchers studied the behaviour of the CFTFGs and developed expressions for the lateral–torsional buckling flexural strength (Kim and Sause 2008). They are appropriate for use in a variety of structural applications, such as bridges, car parks and multi-storey buildings. Generally, because they have very high load-carrying capability, as well as excellent lateral stiffness, they are particularly suitable for large spans and heavily loaded applications. Although they are laterally stable and have high bending strength on their own, they can also act compositely with concrete slabs, connected through traditional shear studs. In this scenario, the slab and some or all of the concrete filled section are likely to act in tension, while the bottom steel flange and web is in tension (depending on the location of the neutral axis). The research of Kim and Sause (2008) was important because a number of significant advantages of utilising CFTFGs relative to conventional I-shaped plate girders were identified, both in service and also during construction:

- It was shown that the torsional stiffness and strength of the girder is significantly increased by the concrete-filled tube, thus increasing the lateral-torsional buckling (LTB) resistance of the girder. This can be particularly important the construction stage when erecting the steel frame or placing the concrete deck.
- The concrete filled tube also has the effect of reducing the depth of the web in compression, thus decreasing the web slenderness. Although some transverse stiffeners are still likely to be required along the girder length to control distortion of the cross-section, the number of stiffeners may be greatly reduced owing to the increased stability and strength of the CFTFG relative to a traditional girder.
- Greater spans can be achieved for the same overall depth, thereby reducing the overall cost and increasing the speed on construction.

Accepted manuscript doi:
10.1680/jstbu.21.00116

- In bridge applications, the improvement in torsional stiffness and strength may eliminates the need for fabricating exterior girders with intermediate constructability stiffeners which are typically required for regular plate girders to resist overhang forces.

It is clearly very important to employ care and attention to ensure that the concrete is properly and fully cast into the steel tube. This is usually ensured by vibrating the concrete thoroughly during the mixing and casting process and also employing a grouting to ensure that there are no gaps between the two materials (Shao and Wang 2017). More recently, both numerical and analytical studies into circular CFTFGs have been conducted, with this work focussing on the fundamental behaviour, including the effects of material and geometric nonlinearity. A series of analytical expressions for predicting the bending capacity of circular CFTFGs were proposed. This study was extended to account for the effects of axial tension applied in combination with bending moments and again, simplified design expressions were proposed (Al-Dujele et al., 2018; Al-Dujele and Cashell 2018, 2019, 2021a, 2021b).

2. Finite element model

A FE model has been developed using the Abaqus software (Simulia 2011) to simulate the behaviour of CFRFG's in bending, and includes the material and geometric nonlinearities present in the response. The model has been developed and validated based on the experiments conducted by Muteb and Ali (2016). This programme included four simply supported specimens, two of which had concrete in the tubular flange (namely CFRFG1 and CFRFG2) and two which were left hollow (SRFG1 and SRFG2). The key dimensions of the test specimens are presented in Table 1 and also shown in Fig. 1, in which B_{Tf} and B_{Bf} are the width of the top and bottom flanges, respectively, D_f is the depth of the top rectangular flange, h_w is the height of the web and t_t, t_f and t_w are the thicknesses of the top rectangular hollow section, the bottom flange plate and the web, respectively. There were six stiffeners along the length of the beam and each was 2.85 mm in thickness ($t_{stiffener}$). These were located at the supports and loading points to prevent local instability of the web at these locations. Furthermore, bearing plates with dimensions 90×80×10 mm are included under each point load to prevent any local buckling in the steel section.

3. Material modelling

3.1 Steel

The stress-strain response of the structural steel is modelled as a bilinear, elastic-linear strain hardening relationship (Muteb and Ali 2016), as shown in Fig. 2(a), where f_y and ε_{st} are the yield stress and strain at the onset of strain hardening, and f_u and ε_u are the ultimate tensile stress and strain at ultimate tensile stress, respectively. In the analysis, the yield stress is taken as 236.8 N/mm^2 and the ultimate strength is given a value of 377.2 N/mm^2. Young's modulus (E_s) and the Poisson's ratio are given values of 200×10^3 N/mm^2 and 0.3, respectively. The strain at the onset of strain hardening (ε_{st}), which is the strain at which the yield stress is reached, and the strain at the ultimate tensile stress (ε_u) are taken as 0.025 and 0.2, respectively, in accordance with the recommendations given by Ban and Bradford (2013). The engineering stress–strain (σ_{eng}-ε_{eng}) curve is converted to true stress–strain (σ_{true}-ε_{true}) curve for the Abaqus model using Eqs (1) and (2):

$$\varepsilon_{true} = \ln(1 + \varepsilon_{eng}) \quad (1)$$

$$\sigma_{true} = \sigma_{eng}(1 + \varepsilon_{eng}) \quad (2)$$

The steel section is represented using four-noded, three-dimensional shell elements with reduced integration (called S4R in the Abaqus library (Simulia 2011)). Following a sensitivity analysis, Simpsons rule with seven integration points is used through the element thickness to determine the response through the section; this provides a good balance between computational efficiency and

accuracy of the results. The S4R element has six active degrees of freedom per node, including three displacements and three rotations. The advantage of the reduced integration elements is that the strains and stresses are calculated at the locations that provide optimal accuracy. A second advantage is that the reduced number of integration points decreases CPU time and storage requirements.

A tie contact is defined between the surface of the steel section and the edges of the stiffeners. Following a mesh sensitivity study, it was determined that an element size of 10×10 mm provides the best combination of accuracy and computational efficiency and therefore is applied to all elements in the model.

3.2 Concrete

The concrete in the tubular flange acts mainly in compression although may be subjected to some degree of transverse loading also, as will be discussed later. Hence, the material relationship for confined concrete in rectangular CFST columns (Liang 2009), as shown in Fig. 2(b), is used. The stress-strain response can be divided into ascending (O-A), constant (A-B), linearly descending (B-C) and constant (C-D) sections. The compressive stress for the ascending part O-A is calculated based on the equations given by Mander et al. (1988):

$$\sigma_c = \frac{\grave{f}_{cc}\,\lambda\,(\varepsilon_c/\varepsilon_{cc})}{\lambda - 1 + (\varepsilon_c/\varepsilon_{cc})^{\lambda}} \quad (3)$$

$$\lambda = \frac{E_c}{E_c - (\grave{f}_{cc}/\varepsilon_{cc})} \quad (4)$$

$$\varepsilon_{cc} = \varepsilon_c\left[1 + 5\left(\frac{\grave{f}_{cc}}{\grave{f}_c} - 1\right)\right] \quad (5)$$

where σ_c is the compressive stress, $\grave{f}_{cc}$ is the effective compressive strength of confined concrete, ε_c is the compressive concrete strain, ε_{cc} is the strain at $\grave{f}_{cc}$ and E_c is the Young's modulus of concrete which is given by the empirical formulation provided in Eurocode 2 (CEN 2004) and given in Eq. (6):

$$E_c = 22 \times (\grave{f}_c/10)^{0.3} \quad (6)$$

In this expression, $\grave{f}_c$ is the unconfined cylinder compressive strength of the concrete and ε_c is the corresponding strain which is determined in accordance with Eurocode 2 Part 1-1 (CEN 2004), as:

$$\varepsilon_c = 0.7(\grave{f}_c)^{0.31} \leq 2.8 \quad (7)$$

When the concrete filled steel tube is exposed to axial compression, a gap occurs between the steel tube and the concrete core in the elastic range because the Poisson's ratio for concrete is less than that of steel. Beyond the elastic range, the inner concrete dilates (strains transversely) at a higher or faster rate than the steel tube, and contact develops again between the steel tube and the concrete. As the axial compressive stress increases further, continued dilation of the concrete core is restricted by the steel tube, generating a variable confining pressure in the concrete in the transverse direction. This confining pressure effectively increases the compressive strength of the concrete core. In a CFRFG, the concrete is confined by the rectangular steel tube section, which results in increased ductility and strength of the concrete core, compared to unconfined concrete.

The effective compressive strength of confined concrete ($\grave{f}_{cc}$) is influenced mainly by the tube size, the quality of concrete and the loading rates. Hence, the value of $\grave{f}_{cc}$ is taken as $\gamma_c \times \grave{f}_c$, where γ_c is the strength reduction factor proposed by Liang (2009) and expressed as:

$$\gamma_c = 1.85 D_c^{-0.135} \; (0.85 \leq \gamma_c \leq 1.0) \quad (8)$$

where D_c is taken as the larger of $B_{Tf} - 2t_t$ and $D_f - 2t_t$ for a rectangular cross-section.

The other regions of the stress–strain curve (i.e. A-B, B-C and C-D in Fig. 2(b)) for confined concrete are defined by the following equations given by Liang (2009):

Accepted manuscript doi:
10.1680/jstbu.21.00116

$$\sigma_c = \begin{cases} \grave{f}_{cc}\grave{f}_{cc} + 100(0.015 - \varepsilon_c)(\grave{f}_{cc} - \beta_c\grave{f}_{cc}) & \text{for } \varepsilon_{cc} < \varepsilon_c \leq 0.005 \\ \beta_c\grave{f}_{cc} + 100(0.015 - \varepsilon_c)(\grave{f}_{cc} - \beta_c\grave{f}_{cc}) & \text{for } 0.005 < \varepsilon_c \leq 0.015 \\ \beta_c\grave{f}_{cc} + 100(0.015 - \varepsilon_c)(\grave{f}_{cc} - \beta_c\grave{f}_{cc}) & \text{for } \varepsilon_c > 0.015 \end{cases} \quad (9)$$

In these expressions, β_c is a constant which accounts for the confinement effect on the concrete ductility and depends on the width-to-thickness ratio (B_s/t_t) of the concrete filled rectangular flange. B_s is taken as the larger of B_{Tf} and D_f for the rectangular flange cross-section. Based on the experimental results presented by Tomii and Sakino (1979), βc is proposed by Liang (2009) to be taken as:

$$\beta_c = \begin{cases} 1.0 & \text{for } B_s/t_t \leq 24 \\ 1.5 - (1/48)(B_s/t_t) & \text{for } 24 < B_s/t_t \leq 48 \\ 0.5 & \text{for } B_s/t_t > 48 \end{cases} \quad (10)$$

The softening behaviour of concrete in the post-yield stage is determined by the β_c parameter and the concrete strain (ε_{cu}). The values of β_c determined using Eq. (10) account for the effect of the B_s/t_t ratio of the steel tube on the softening of the concrete.

The concrete infill is represented using 8-noded solid elements with reduced integration, known as C3D8R in the Abaqus library. The concrete damaged plasticity (CDP) model is employed to describe the constitutive behaviour of the material. To represent the inelastic behaviour, the CDP model uses the concept of isotropic damaged elasticity, in combination with isotropic tensile and compressive plasticity. It is assumed that the uniaxial tensile and compressive behaviours are characterized by damaged plasticity. The plasticity parameters required by the CDP model are the dilation angle, eccentricity, ratio of the strength in the triaxial state to that in the uniaxial state and the K parameter and these are taken as 36°, 0.1, 1.16 and 0.667, respectively, in the current work (Kmiecik and Kamiński 2011). A tie constraint is used between the steel tube as the master surface and the infilled concrete as the slave surface. The interface between the steel tube and concrete infill for the FE models of the confined concrete was modelled as a rigid connection, and therefore it is assumed that there is perfect bond between the two constituent materials. This was shown to be the case, and therefore a legitimate assumption, during a previous study by Kim and Sause (2008). Generally, the target and contact surface were determined based on the stiffness of materials. Since the Young's modulus of steel is significantly larger than that of concrete, the steel surface is defined as the target surface, while the concrete surface is the contact surface.

3.3 Boundary conditions, load application, initial imperfections and solution procedure

Owing to symmetry of the geometry and loading conditions about the mid-span, only half the girder is modelled in Abaqus. Therefore, one end section of the model has simply supported boundary conditions and the other end section, representing the mid-span, has symmetrical boundary conditions. The boundary conditions used for the half-length FE models are shown in Fig. 3, in which u_x, u_y, u_z, θ_x, θ_y, and θ_z are the displacements and the rotations about the global x, y and z axes, respectively. The y-z plane is considered to be in-plane whereas the x-z and x-y planes are out-of-plane.

The implicit dynamic analysis method is employed to simulate the response, accounting for the geometric and material nonlinearities. The load is applied incrementally and the nonlinear geometry parameter (NLGEOM) is included for the large displacement analysis. This nonlinear dynamic analysis method uses an implicit time integration scheme to calculate the transient dynamic or quasi-static response of a system, which is found in the current study to provide the best convergence

behaviour owing to the high energy dissipation associated with quasi-static applications during certain stages of the loading history. The loading is applied to the top surface of the beam in displacement control through two concentrated loads along the full length or one loading point when half the span is considered.

As with all steel sections, initial imperfections are likely to be present in the member following manufacturing. The initial imperfections are considered in the model and are obtained as the first eigenmode during an elastic buckling eigenvalue analysis; these are then added to the initially perfect geometry in terms of shape and amplitude. The imperfection is assumed to has an amplitude of L/1000, where L is the member length, in accordance with the permitted out-of-straightness tolerance in EN 1090-2 (CEN 2008). For a CFRFG, buckling takes place in a lateral-torsional mode as the web becomes stiffened transversally at the mid-span, causing lateral buckling to control rather than the web distortions, as shown in Fig. 9. On the other hand, residual stresses are not included in the current analysis in order to minimise complexity in the model, based on the findings in similar studies (Dong and Sause 2009).

3.4 Validation of the FE model

The accuracy of the FE model is assessed by analysing four different test specimens available in the literature (Muteb and Ali 2016) and comparing the published results with those obtained from the FE model. The load-displacement response for both the concrete filled and the hollow rectangular flange girders are presented in Fig. 4. The ultimate load obtained from the FE analysis ($P_{u,FE}$) is presented together with the corresponding test value ($P_{u,Exp}$) in Table 1, which also includes the ratio of $P_{u,FE}$ to $P_{u,Exp}$. From Fig. 4, it can be seen that a good agreement is achieved between the experimental and finite element modelling results. Initially, at the start of the experiment, there was an initial increase in deflection in the experimental responses, which is likely due to some movement or tolerance in the experimental arrangement, and this was not reflected in the numerical model. The overall shapes of the responses are very similar between the experimental and numerical results. There are some relatively minor disparities between the experimental and numerical load capacity of the beams, and these are likely due to a combination of factors such as the idealisation of material behaviour and nonlinearity in the FE model, hardening of the steel during the experiment and as well as the likelihood of initial imperfections in the real structure.

4. Analytical design method

In this section, an analytical procedure for estimating the flexural strength of CFRFGs is presented, based a fundamental assessment of the structural behaviour. Theoretical equations are derived based on plastic theory, in which the location of the plastic neutral axis (PNA) and the flexural strength can be determined by equilibrating the internal forces in the member. The model adopts equivalent stress blocks to represent the stress distribution in the steel and concrete and the confining effect provided by the steel tube to the concrete infill is also considered. The accuracy of the approach is examined by comparing the predictions of the equations with the FE results.

Two different cases are presented, depending on the location of the plastic neutral axis (PNA), as shown in Fig 5. Case 1 is presented in Fig. 5(a) and it is assumed that the PNA is in the web of the steel section while Case 2, as shown in Fig 5(b), assumes that the PNA is in the tubular flange. In order to determine the exact location of the PNA, the following assumptions are adopted, with reference to the distributions and terms defined in Fig. 5:

- The term y_2, which is the vertical height of the triangular stress block is determined by interpolating the strain distribution across the cross-section, given by:

Accepted manuscript doi:
10.1680/jstbu.21.00116

$$\frac{\varepsilon_{cc}}{y_1 - t_t} = \frac{\varepsilon_y}{y_2} \rightarrow y_2 = \frac{\varepsilon_y}{\varepsilon_{cc}}(y_1 - t_t)$$

- In the triangular stress block, where the steel is behaving in an elastic manner (i.e. $f_s = \varepsilon_s E_s$, where f_s and ε_s are the stress and strain in the steel section, respectively, and E_s is the elastic modulus), interpolation can be applied to establish that, at any location y in this region, the stress in the steel is determined as:

$$f_s = \frac{y f_y}{y_2}$$

In these expressions, y is any location the region, y_1 is the distance from the PNA to the top of the girder whilst y_2 is the vertical height of the triangular stress block. For Case 1, $y_1 > D_f$ (where D_f is the depth of the steel tube), and therefore the PNA is within the steel web. On the other hand, for Case 2, $y_1 < D_f$, and the PNA is within the concrete filled tube. The plastic moment for these two cases can be determined as described hereafter.

Case 1: PNA is in the web section ($y_1 > D_f$)

Fig. 5(a) presents the strain and stress distributions through the cross-section for Case 1, where the PNA is in the web of the steel section ($y_1 > D_f$). The internal axial force for each component of the section can be computed as shown in Table 2. The location of the PNA (y_1) for this case can be determined by applying the equilibrium of axial force condition, expressed in Eq. 11:

$$C_c + C1_{tf} + C2_{tf} + C_w = T1_w + T2_w + T1_f \qquad (11)$$

The ultimate moment (M_u) of the CFRFG section can then be calculated according to Eq. 12:

$$M_u = (C_c + C1_{tf} + C2_{tf}) \times y + C_w \times \frac{2}{3}(y_1 - D_f) + T1_w \times \frac{2}{3}y_2 + T2_w \times \frac{(h - y_1 - y_2 - t_w)}{2} + T1_f \times (h - y_1 - \frac{t_f}{2}) \qquad (12)$$

Case 2: PNA is in the tubular rectangular flange section ($y_1 < D_f$)

The internal axial force for each component of the section can be computed using the expressions presented in Table 2. The strain and stress distributions for Case 2 are given in Fig. 5(b), where it is shown that the PNA is in the tubular flange section ($y_1 < D_f$). It is assumed that the concrete below the PNA does not contribute to the tension capacity. The location of the PNA for this case can be determined from the equilibrium of axial forces, given as:

$$C_c + C1_{tf} + C2_{tf} = T_{tf} + T1_w + T2_w + T1_f \qquad (13)$$

Then, the ultimate moment (M_u) of the CFRFG section can be calculated as:

$$M_u = (C_c + C1_{tf} + C2_{tf} + T_{tf} + T1_w) \times y + T2_w \times ((h - y_1 - y_2 - t_w)/2 + (y_2)) + T1_f \times (t_f/2 + (h - y_1 - y_2 - t_f) + (y_2)) \qquad (14)$$

In the equations presented in Tables 2 $C1_{tf}$ and $C2_{tf}$ represent the rectangular and triangular stress blocks for the compressive forces in the tubular flange, respectively. $T1_w$ and $T2_w$ denote the triangular and rectangular stress blocks for the tensile forces in the steel web below PNA, respectively, and σ_c is the stress in the confined concrete obtained using Eq. 3 earlier in this paper.

The analytical model has been applied to the four test beams (Muteb and Ali 2016) used before for the FE model validation, and the results are presented in Table 3. The ultimate moment capacity predicted using the analytical approach is denoted as $M_{u,Calc}$ whilst the corresponding value from the Abaqus model and experimental test is $M_{u,FE}$ and $M_{u,Exp}$, respectively. In terms of analytical moment, the PNA is found to be in the web of the steel section for all of these beams and the formulations for Case 1 are

therefore used. The results show that this depth of the PNA from the top of the steel sections is 37.1 and 49.4 mm for CFRFG1 and CFRFG2, respectively. On the other hand, for the similar members without concrete infill, y_1 is 66.7 mm and 71.8 mm for SRFG1 and SRFG2, respectively. It is clear from the results in the table, particularly, the $M_{u,FE}$ to $M_{u,Calc}$ ratio, that the analytical approach provides a good prediction of the moment capacity for these beams, particularly for the concrete filled specimens. In this case, there is only 6% difference between the FE predictions and the capacities predicted by the simplified analytical approach. The values indicate the accuracy of the analytical expressions in predicting the ultimate moment as, in all cases, the $M_{u,FE}/M_{u,Calc}$ ratio is between 0.89 and 0.99.

5. Parametric study

The parameters studied are presented in Tables 4 and 5 witches include various geometric properties such as tube thickness, depth and width as well as the thickness and depth of the web and the tension flange width and thickness. For ease of visualisation, the results are presented in two general categories. Firstly, as shown in Tables 4(a) and (b), members with different rectangular tube dimensions (D_f = 20, 22.3, 40 or 42.3 mm), web height (h_w taken as either 127, 147 or 250 mm), width of the bottom flange (B_{Bf} = 80 or 120 mm), thickness of the steel section (t_{beam} = 2.85 or 4 mm) and cross-sectional aspect ratios (a/h_w= 5.0, 4.4 or 2.6) are presented for both CFRFGs (Table 4) and identical members without the concrete infill, i.e. SRFGs (Table 4(b)). In this study, two different width-to-depth ratios (B_{Tf}/D_f =2 or 4) are studied. Tables 5(a) and (b) present the other parameters varied in the study, with the main focus being on the influence of steel section thickness of the various individual plate components (t_t, t_w and t_f), for CFRFGs and SRFGs respectively.

In all cases, the webs of the girders are reinforced with double-sided flat plate stiffeners, which are 2.85 mm in thickness, and located at the support and loading points. The distance (a) between the two intermediate stiffeners, as shown in Fig. 3, is 640 mm. All beams are 2020 mm in length. The specimens listed in Tables 4(a) and 5(a) are filled with concrete which has a compressive strength of 42.5 MPa. It is noteworthy that when studying the effect of steel section thickness (which is varied between 2.85 and 4 mm in this study), the area of concrete remains constant at either 2548.5 mm^2 or 1062.5 mm^2 for (D_f =20 or 40 mm), respectively. It is noted that during the FE simulation as well as experimental programme (Muteb and Ali 2016), the failure mode for all specimens considered is high levels of deflection, i.e. serviceability failure. The members with no concrete also exhibit local buckling of the compression flange. Accordingly, in the current study, an allowable deflection limit of span/250 is considered as given in National Annex of Eurocode 3 (2005). In addition, all of the sections in the current study were examined for local buckling using the tube slenderness limit provided by the AASHTO LRFD specifications (1999) for rectangular tubular compression members, given in Eq. 15:

$$\frac{B_{Tf}}{t_t} \leq 1.7\sqrt{\frac{E_s}{f_y}} \quad (15)$$

This expression was originally developed for unfilled tubes, although the AASHTO specification now recommends using this check for filled concrete tubes also.

The ultimate moments determined using the FE model ($M_{u,FE}$) and the analytical expressions ($M_{u,Calc}$) are shown in Tables 4 and 5 together with the location of the PNA measured from the top of the section (y_1). Each pair of CFRFGs and SRFGs had similar buckling forms, but the buckling resistance of the concrete filled members is higher than the corresponding SRFGs. For example, with reference

to Tables 4 (a) and (b), $M_{u,FE}$ is higher for GR1 (18.7 kNm) than GR17 (15.0 kNm) which are identical apart from the presence of the concrete infill in GR1. This corresponds to a 25% increase in capacity due to the presence of concrete in the tube, which increases the strength and rigidity of the upper flange and therefore allows additional loads to be carried by the concrete filled section. The load deflection and failure behaviour of both CFRFGs and SRFGs with different key parameters are described and discussed in detail in the following sub-sections.

5.1 Geometry of the tubular flange

The effect of a number of the most salient individual geometric properties such as rectangular tube depth (D_f), width (B_{Tf}) and thickness (t_t) are studied herein. Two different width-to-depth ratios (B_{Tf}/D_f) for the compression infilled concrete tubular flange are assessed. With reference to Fig. 6, the results indicate that reducing the aspect ratio of the flange has the effect of increasing the flexural capacity of the CFRFGs. The data in Tables 4 (a) shows that the ultimate moment for GR8 (B_{Tf}/D_f =4) is 60.4 kNm while the same value for GR16 (B_{Tf}/D_f =2) is 66.2 kNm. Similarly, the ultimate moment for GR24 (SFRG with B_{Tf}/D_f =4) is 52.8 kNm while $M_{u,FE}$ for GR32 (B_{Tf}/D_f =2) is 58.9 kNm. This demonstrates that the contribution to the overall flexural strength that is made by the tubular flange increases as the B_{Tf}/D_f ratio decreases.

The moment-deflection responses for (a) CFRFGs and (b) SRFGs are shown in Fig. 6 and it is clear that decreasing the B_{Tf}/D_f ratio increases the ultimate flexural strength of the girder. The initial stiffness of the moment-deflection response is greater for members with a relatively lower B_{Tf}/D_f ratio. On the other hand, since increasing the flange depth (D_f) leads to an increase in the CFRFG's entire cross-sectional area, it is important to assess the additional flexural strength of the girder which can be obtained. The rectangular tubular flange depth variation from 20 mm to 40 mm increases the cross-sectional steel area by around 8% (i.e. the total area for GR3 is 1478 mm^2 whereas it is 1592 mm^2 for GR11). These two beams have an ultimate moment capacity of around 37.7 kNm and 43.1 kNm for GR3 and GR11, respectively. Therefore, an 8% increase in the volume of steel can lead to a 15% increase in the bending moment capacity.

Two different tube thicknesses (t_t) are examined in this study, i.e. 2.85 mm and 4 mm. A general conclusion is that increasing the thickness of the steel tube increases the ultimate moment for CFRFGs and SRFGs, as expected. For example, the ultimate moments are 20.1 and 21.8 kNm for GR9 (t_t=2.85 mm) and GR45 (t_t=4 mm), respectively. This improves the strength and stiffness of the compression flange and allows a 9% increase in capacity. The results show an improvement in moment when increase the steel thickness of the tube with constant area of concrete. In addition, Tables (4 and 5) present the variation of $M_{u,FE}/M_{u,Calc}$ for different groups of CFRFGs and SRFGs. The values indicate the accuracy of the analytical expressions in predicting the ultimate moment as, in all cases, the $M_{u,FE}/M_{u,Calc}$ ratio is between 0.89 and 0.99.

5.2 Geometry of the steel web

Firstly, the effect of the aspect ratio of the girder web panel (a/h_w) is examined. As previously noted in Tables 5 (a) and (b), a reduction of the aspect ratio of the web panels for the girders with otherwise identical geometries leads to an increase in the ultimate moment capacity of the member. Fig. 7 shows the ultimate moment-deflection curves for both types of girder and highlights the differences in their general behaviour. After the linear elastic stage and until the full strength of the girders is reached, the girder with the higher web panel aspect ratio (GR6) reaches the inelastic stress stage at a lower deflection relative to GR8 and also achieves a considerably higher flexural capacity. After that point, the response plateaus as the displacement continues to increase with very little change in the flexural

capacity. It is shown that the initial stiffness of the response in the elastic range is greater for the members with a relatively lower aspect ratio.

In order to illustrate the general behaviour of SRFGs without a concrete infill, the moment-deflection curves of GR22 and GR24 are plotted in Figs. 7(b). These are identical to GR6 and GR8 mentioned above apart from having a hollow top flange. Generally, the behaviour of GR22 and GR24 are quite similar to GR6 and GR8, although the capacities are lower as expected. It is noteworthy that the capacity decreases more rapidly for the hollow members compared with the CFRFGs after the peak moment has been reached. In addition, it is shown that for members with a relatively high aspect ratio (i.e. GR6 and GR22), their ultimate bending moments are 32.7 and 27.5 kNm, respectively, representing a difference of 16%. On the other hand, the same values for GR8 and GR24 are 60.4 and 52.8 kNm, giving a difference of 12%. This show that the influence of the concrete infill is more pronounced for beams with a larger aspect ratio (i.e. GR6 and GR22).

With reference to the data presented in Tables 4 and 5, it can be seen that increasing the web thickness leads to an improvement of the flexural strength. This is evidenced by comparing GR1 (t_w=2.85 mm) with GR34 (t_w=4 mm), for example. These two beams have an ultimate moment capacity of around 18.7 kNm and 21.8 kNm, respectively, and a gross cross-sectional area (steel only) of 1185 and 1354 mm^2, respectively. Therefore, a 14% increase in steel volume results in a 17% improvement in bending moment capacity, for the same stiffener arrangement.

Similarly, it is observed in the data presented in Tables 4 and 5 that an increase in the web height (h_w) leads to a greater increase in the moment capacity of the CFRFGs and SRFGs, as expected. For CFRFGs, the ultimate moment of GR1 (h_w=147 mm) is 18.7 kNm, for example, whereas $M_{u,FE}$ for GR3 (h_w=250 mm) is 37.7 kNm. The effect of web height is further studied in Fig. 8 for two specimens with a web height of either 127 or 250 mm. It is observed that the initial stiffness of the curves is greater when h_w is relatively higher. Clearly, decreasing the web depth (h_w) reduces the volume of steel in the section as well as the fabrication costs as less welding is required and the associated risk of weld distortion is lowered. However, it also reduces the bending moment capacity. Therefore, this discussion highlights the importance of a careful consideration of all factors (capacity requirements, flange depth, web depth, welding needs, etc.) when designing these types of members.

5.3 Geometry of the bottom flange

The effect that the width of the bottom flange (B_{Bf}) has on the structural behaviour of the CFRFGs and SRFGs is observed in Fig. 9(a) and (b), respectively. Two different flange widths have been studied, namely 80 and 120 mm. It is clearly shown in the figures that a wider tension flange results in a greater second moment of area for the section and therefore increases the ultimate flexural strength. Accordingly, and as expected, the flexural capacity of both CFRFGs and SRFGs increases for greater tension flange widths (B_{Bf}). As demonstrated in Fig. 9, and also the data in Tables 4 and 5, the increase in flexural capacity from GR9 and GR25, for the CFTFG and SRFG with a bottom flange width of 80 mm, to GR13 and GR29, which were identical except having a bottom flange width of 120 mm, is 19% and 20%, respectively, although the increase in steel area is only 9% (the total steel area in GR9 and GR25 was 1242 mm^2 whereas the same value for GR13 and GR29 is 1355.5mm^2).

The influence of bottom flange thickness (t_f) on the capacity of the section is also investigated. With reference to Tables 4and 5, for example, the ultimate moment of GR13 (t_f=2.85 mm) is 23.9 kNm whereas the same value for GR50 (t_f=4 mm) is 28.8 kNm. On the other hand, for equivalent SRFGs, these values are 19.6 kNm and 23.1 kNm for GR29 (t_t=2.85 mm) and GR74 (t_t=4 mm), respectively. Thus, changing the bottom flange thickness from 2.85 mm to 4 mm thereby increasing the total steel cross-sectional area by 9%, results in an improved moment capacity of almost 21% and 18% for

CFRFGs and SRFGs, respectively. It is worth noting that the design of the cross-sectional properties must be carefully considered in terms of optimum thickness and width, relative to the required moment capacity, in order to provide an efficient and economical design both in terms of material and fabrication costs.

6. Conclusions

In this paper, the flexural behaviour of concrete filled rectangular flange girders (CFRFGs) is presented and assessed. Two different analysis techniques are developed including a numerical finite element model, developed in Abaqus (Simulia 2011), and also an analytical method based on the material and geometrical properties, using a plastic analysis approach. The finite element model has been validated using available experimental data and is shown to provide an accurate and reliable simulation of the response. The analytical model is particularly aimed at designers, and it is very simple to apply. Following validation, both the numerical and the analytical models are employed in this paper to conduct a detailed parametric study in order to identify and quantify the most salient and influential properties, both in terms of the flexural capacity and the overall behaviour. The key variables studied include the geometry of the different components (i.e. the compression tubular compression flange, web and bottom tension flange) and also the material strengths. The results also are compared with steel rectangular flange girders (SRFGs) which do not have the concrete infill to thoroughly investigate the difference in flexural behaviour between both types of girder. Based on the investigation, the following concluding remarks are presented:

- The analysis of the results indicate that reducing the aspect ratio of the tubular flange (B_{Tf}/D_f) increases the flexural strength of the girders.
- The CFRFGs and SRFGs had similar buckling shapes, with the CFRFGs achieving greater buckling loads than those of the corresponding SRFGs. This emphasizes the influence of the concrete infill which increases the stiffness of the upper flange and thus makes it possible for the web to carry greater moments, compared with SRFGs.
- The flexural strengths predicted using the simplified analytical expressions show that the capacity of both CFRFGs and SRFGs is accurate and slightly conservative.
- In terms of the geometrical details, increasing the depth of the tensile flange (t_f) is shown to be advantageous for both the moment capacity and the material costs. This is because it increases the ultimate moment capacity of the girder to a more significant extent than the increase in material cross-sectional area.
- It has been shown clearly that a decrease in the aspect ratio of the web panel (a/h_w) results in an increase in the bending strength of the girders. Such an increase is greater for CFRFGs compared with SRFGs. It can also be concluded that it is more significant and beneficial to increase the depth of the infilled tubular flange ($D_{f)}$ rather than decreasing the web panel aspect ratio (a/h_w) for girders that are formed from a relatively small top flange depth. Hence, design engineers should firstly work on checking the CFRFGs formed from compression tubular flanges with relatively smaller width-to-depth ratios (B_{Tf}/D_f) and relatively big web panel aspect ratios (a/h_w) before considering larger flanges with relatively smaller aspect ratios (a/h_w).
- In view of the absence of any suitable design expression in Eurocode 4 (CEN 2004), the analytical design model which is developed in this paper provides appropriate predictions for the capacity of CFRFGs under bending. The model is based on a fundamental behavioural assessment which reveals the relative influence of material and geometric parameters.

- Finally, it is clear from the analysis presented in this paper that concrete filled tubular flange girders are a promising cross-section for heavily-loaded structural applications, providing both efficiency in terms of material usage and effectiveness in carrying large forces and moments.

Acknowledgments

The authors would like to gratefully acknowledge the financial support by the Office of the Prime Minister of Iraq through the Higher Committee for Education Development in Iraq.

Notation

The following symbols are used in this paper:

a Distance between the simple support and the vertical force
A_s Cross-sectional area of the steel
B_{Bf} Width of the bottom flange
B_{Tf} Width of the rectangular tube flange
D_f Depth of the rectangular tube
d_c The compressive damage parameter
d_t The tensile damage parameter
E_c Modulus of elasticity of concrete
E_s Modulus of elasticity of structural steel
$\grave{f}_c$ Uniaxial compressive cylinder strength of unconfined concrete at 28 days
$\grave{f}_{cc}$ Uniaxial compressive cylinder strength of confined concrete at 28 days
f_t The tensile strength of concrete
f_u Ultimate strength of structural steel
f_y Yield strength of structural steel
h_w Web depth
L Member length
M_u Ultimate bending capacity of a CFRFG in pure flexure
$M_{u,Exp}$, $M_{u,Calc}$ and $M_{u,FE}$ The experimental, calculated and FE ultimate moment capacity, respectively
$P_{u,Exp}$, $P_{u,FE}$ Ultimate experimental and FE load, respectively
t_{beam}, t_t, t_w, t_f, $t_{stiffener}$ Thickness of the steel beam section, tube, web, bottom flange, stiffener, respectively.
u_x, u_y and u_z Displacements about the global x, y and z axes, respectively.
x_0, y_0 Center of the rectangular tube
y_1 Predicting the location of the PNA from the top of the girder
y_2 The vertical height of the triangular stress block
ε Strain
ε_c Unconfined concrete strain at peak stress
ε_{cc} Confined concrete strain at peak stress
ε_{eng} Engineering strain

ε_{true} True strain
ε_u Ultimate strain of structural steel at break
σ Stress
σ_c Uniaxial compression yield stress of concrete
σ_{eng} Engineering stress
σ_{true} True stress
θ_x, θ_y and θ_z Rotations about the global x, y and z axes, respectively.

References

AASHTO. 1999. "AASHTO LRFD Bridge Design Specifications." American Association of State Highway and Transportation Officials, Washington, DC.

Al-Dujele, R., Cashell, K.A. and Afshan, S., 2018. Flexural behaviour of concrete filled tubular flange girders. Journal of Constructional Steel Research, 151, pp.263-279.

Al-Dujele, R. and Cashell, K.A. 2018. "The effects of axial tension on the sagging-moment regions of concrete-filled tubular flange girders." Proceedings of 9th International Conference on Advances in Steel Structures (ICASS), Hong Kong, China.

Al-Dujele, R. and Cashell, K.A., 2019. An evaluation of the flexural behaviour of concrete-filled rectangular flange girders. Proceedings of 9th International Conference on Steel and Aluminium Structures (ICSAS), Bradford, UK.

Al-Dujele, R. and Cashell, K.A., 2021a. Design and analysis of concrete-filled tubular flange girders under combined loading. Advances in Structural Engineering, 24(11), pp.2512-2528.

Al-Dujele, R. and Cashell, K.A., 2021b. Behaviour of rectangular concrete filled tubular flange girders under combined loading. ce/papers, 4(2-4), pp.551-557.

Avery, P. and Mahendran, M. 1997. "Finite-element analysis of hollow flange beams with web stiffeners." ASCE Journal of Structural Engineering, 123(9), pp.1123-1129.

Anapayan, T., Mahendran, M. and Mahaarachchi, D. 2011. "Section moment capacity tests of LiteSteel beams." Thin-Walled Structures, 49(4), pp.502-512.

Ban, H. and Bradford, M.A. 2013. "Flexural behaviour of composite beams with high strength steel." Engineering Structures, 56, pp.1130-1141.

CEN (European Committee for Standardization). 2004. "Design of Concrete Structures: General Rules and Rules for Buildings, Part 1.1." Eurocode 2, Brussels.

CEN (European Committee for Standardization). 2004. "Design of Composite Steel and Concrete Structures: General Rules and Rules for Buildings, Part 1.1." Eurocode 4, Brussels.

CEN (European Committee for Standardization). 2008. "Execution of Steel Structures and Aluminium Structures–Part 2: Technical Requirements for Steel Structures." EN 1090 Part 2, Brussels.

Chung, K.F. and Lawson, R.M. 2001. "Simplified design of composite beams with large web openings to Eurocode 4." Journal of Constructional Steel Research, 57(2), pp.135-164.

Dong, J. and Sause, R. 2009. "Flexural strength of tubular flange girders." Journal of Constructional Steel Research, 65(3), pp.622-630.

Ge, H. and Usami, T. 1992. "Strength of concrete-filled thin-walled steel box columns: experiment." ASCE Journal of structural engineering, 118(11), pp.3036-3054.

Keerthan, P. and Mahendran, M. 2010. "Elastic shear buckling characteristics of LiteSteel beams." Journal of Constructional Steel Research, 66(11), pp.1309-1319.

Kim, B.G. and Sause, R. 2008. "Lateral torsional buckling strength of tubular flange girders." ASCE Journal of structural engineering, 134(6), pp.902-910.

Kmiecik, P. and Kamiński, M. 2011. "Modelling of reinforced concrete structures and composite structures with concrete strength degradation taken into consideration." Archives of civil and mechanical engineering, 11(3), pp.623-636.

Liang, Q.Q. 2009. "Performance-based analysis of concrete-filled steel tubular beam–columns, Part I: Theory and algorithms." Journal of Constructional Steel Research, 65(2), pp.363-372.

Mander, J.B., Priestley, M.J. and Park, R. 1988. "Theoretical stress-strain model for confined concrete." Journal of structural engineering, 114(8), pp.1804-1826.

Mahendran, M. and Mahaarachchi, D.P. 2006. "Development, Behaviour and Design of LiteSteel Beams." Proceedings of 4th International Symposium on Steel Structures, pp. 943–51.

Mollazadeh, M.H. 2015. "Load Introduction into Concrete-Filled Steel Tubular." Doctoral dissertation, The University of Manchester, UK.

Muteb, H. and Ali, A. 2016. "Experimental and Finite Element Analysis of Lateral Torsional Buckling of Concrete Filled Tubular Flange Steel Girders." Journal of Civil and Environmental Research, Vol.8, No.4.

NA of BS EN 1993-1-1. 2005. "Design of Steel Structures Part 1.1: General rules and rules for buildings." National Annex to Eurocode 3, UK.

Pi, Y.L. and Trahair, N.S. 1997. "Lateral-distortional buckling of hollow flange beams." ASCE Journal of Structural Engineering, 123(6), pp.695-702.

Seo, J.K. and Mahendran, M. 2011. "Plastic bending behaviour and section moment capacities of mono-symmetric LiteSteel beams with web openings." Thin-Walled Structures, 49(4), pp.513-522.

Shao, Y. and Wang, Y., 2017. Experimental study on static behavior of I-girder with concrete-filled rectangular flange and corrugated web under concentrated load at mid-span. Engineering Structures, 130, pp.124-141.

Simulia, 2011. ABAQUS Theory Manual. Version 6.14-4, Dassault Systems. `

Tomii, M. and Sakino, K. 1979. "Elasto-plastic behavior of concrete filled square steel tubular beam-columns." Transactions of the Architectural Institute of Japan, 280, pp.111-122.

Table 1 Details of the CFRFG cross-sections for analysis

Specimen	B_{Tf} (mm)	D_f (mm)	t_t (mm)	h_w (mm)	t_w (mm)	B_{Bf} (mm)	t_f (mm)	$t_{stiffener}$ (mm)	$P_{u,Exp}$ (kN)	$P_{u,FE}$ (kN)
CFRFG1	80	20	2.85	147.15	2.85	80	2.85	2.85	73.5	74.2
CFRFG2	80	40	2.85	127.15	2.85	80	2.85	2.85	71.0	71.4
SRFG1	80	20	2.85	147.15	2.85	80	2.85	2.85	61.1	61.4
SRFG2	80	40	2.85	127.15	2.85	80	2.85	2.85	58.0	59.7

Accepted manuscript doi:
10.1680/jstbu.21.00116

Table 2 Internal force components for analytical model

Internal axial force component	(Case 1) Force equation in case the PNA exists at the web	(Case 2) Force equation in case the PNA exists at the tubular rectangular flange
Compression force at infilled concrete (C_c)	$\int_{y_1-D_f+t_t}^{y_1-t_t} (B_{Tf}-2t_t)\times \sigma_c dy$	$\int_{0}^{y_1-t_t} (B_{Tf}-2t_t)\times \sigma_c dy$
Compression force at tubular flange ($C1_{tf}$)	$2\int_{y_2}^{y_1-t_t} t_t \times f_y dy + \int_{y_1-t_t}^{y_1} B_{Tf} \times f_y dy$	$\int_{y_1-t_t}^{y_1} B_{Tf}\times f_y dy + 2\int_{y_2}^{y_1-t_t} t_t \times f_y dy$
Compression force at tubular flange ($C2_{tf}$)	$2\int_{y_1-D_f+t_t}^{y_2} t_t \times f_s dy + \int_{y_1-D_f}^{y_1-D_f+t_t} B_{Tf} \times f_s dy$	$2\int_{0}^{y_2} t_t \times f_s dy$
Compression force at web above PNA (C_w)	$\frac{1}{2}t_w \times (y_1-D_f)\times \frac{f_y(y_1-D_f)}{y_2}$	———
Tension force at web below PNA ($T1_w$)	$\frac{1}{2}\times t_w \times y_2 \times f_y$	$\int_{-y_2}^{y_1-D_f} t_w \times f_s d_y$
Tension force at web below PNA ($T2_w$)	$t_w \times (h-y_1-y_2-t_w)\times f_y$	$(h-y_1-y_2-t_w)\times t_w \times f_y$
Tension force at tubular flange below PNA (T_{tf})	———	$2\int_{-(D_f-t_t-y_1)}^{0} t_t \times f_s dy + \int_{-(D_f-y_1)}^{-(D_f-t_t-y_1)} B_{Tf} \times f_s dy$
Tension force at lower flange (T_{lf})	$B_{Bf}\times t_f \times f_y$	$B_{Bf}\times t_f \times f_y$

Table 3 Comparisons of experimental, numerical and analytical ultimate strengths

Specimen	$M_{u,Exp}$ (kNm)	$M_{u,FE}$ (kNm)	$M_{u,Calc}$ (kNm)	y_1 (mm)	$M_{u,FE}/M_{u,Calc}$
CFRFG1	23.5	18.7	19.9	37.1	0.94
CFRFG2	22.7	20.1	20.8	49.4	0.96
SRFG1	19.6	15.0	16.9	66.7	0.89
SRFG2	18.6	16.4	17.3	71.8	0.95

Accepted manuscript doi:
10.1680/jstbu.21.00116

Table 4 (a) Details of CFRFGs with different tubular flange depths

CFRFG Group	Specimen	Geometric details							$M_{u,FE}$ (kNm)	$M_{u,Calc}$ (kNm)	PNA location, y_1 (mm)	$M_{u,FE}$ / $M_{u,Calc}$	As (mm^2)
		t_{beam}	D_f	B_{Tf}	B_{Bf}	h_w	a/h_w	B_{Tf}/D_f					
G1	GR1	2.85	20	80	80	147	4.4	4	18.7	19.9	37.1	0.94	1185.0
	GR2	4	22.3	82.3					26.8	27.6	38.5	0.97	1681.4
	GR3	2.85	20	80		250	2.6		37.7	39.5	74.4	0.95	1478.0
	GR4	4	22.3	82.3					53.1	54.5	74.8	0.97	2092.8
G2	GR5	2.85	20	80	120	147	4.4		22.9	23.8	49.3	0.96	1299.0
	GR6	4	22.3	82.3					32.7	33.9	50.4	0.96	1841.4
	GR7	2.85	20	80		250	2.6		43.2	44.6	92.8	0.97	1592.0
	GR8	4	22.3	82.3					60.4	61.4	93.1	0.98	2252.8
G3	GR9	2.85	40	80	80	127	5.0	2	20.1	20.8	49.4	0.96	1242.0
	GR10	4	42.3	82.3					28.3	29.2	50.9	0.97	1761.4
	GR11	2.85	40	80		250	2.6		43.1	44.8	87.0	0.96	1592.0
	GR12	4	42.3	82.3					57.3	58.9	89.2	0.97	2252.8
G4	GR13	2.85	40	80	120	127	5.0		23.9	25.0	59.5	0.96	1355.5
	GR14	4	42.3	82.3					33.6	35.1	60.7	0.96	1921.4
	GR15	2.85	40	80		250	2.6		49.5	50.4	102.5	0.98	1706.0
	GR16	4	42.3	82.3					66.2	67.0	103.1	0.99	2412.8

Table 4 (b) Details of SRFGs with different tubular flange depths

SRFG Group	Specimen	Geometric details							$M_{u,FE}$ (kNm)	$M_{u,Calc}$ (kNm)	PNA location, y_1 (mm)	$M_{u,FE}$ / $M_{u,Calc}$	As (mm^2)
		t_{beam}	D_f	B_{Tf}	B_{Bf}	h_w	a/h_w	B_{Tf}/D_f					
G5	GR17	2.85	20	80	80	147	4.4	4	15.0	16.9	66.7	0.89	1185.0
	GR18	4	22.3	82.3					22.4	24.7	67.6	0.91	1681.4
	GR19	2.85	20	80		250	2.6		32.9	35.1	92.5	0.94	1478.0
	GR20	4	22.3	82.3					47.3	49.4	93.4	0.96	2092.8
G6	GR21	2.85	20	80	120	147	4.4		18.4	19.6	76.3	0.94	1299.0
	GR22	4	22.3	82.3					27.5	29.2	77.9	0.94	1841.4
	GR23	2.85	20	80		250	2.6		37.9	40.0	102.7	0.95	1592.0
	GR24	4	22.3	82.3					52.8	55.1	103.6	0.96	2252.8
G7	GR25	2.85	40	80	80	127	5.0	2	16.4	17.3	71.8	0.95	1242.0
	GR26	4	42.3	82.3					23.3	24.3	72.9	0.96	1761.4
	GR27	2.85	40	80		250	2.6		36.0	36.9	102.5	0.97	1592.0
	GR28	4	42.3	82.3					52.2	53.2	103.8	0.98	2252.8
G8	GR29	2.85	40	80	120	127	5.0		19.6	19.8	81.4	0.98	1355.5
	GR30	4	42.3	82.3					27.8	28.0	82.3	0.99	1921.4
	GR31	2.85	40	80		250	2.6		41.7	42.1	110.7	0.99	1706.0
	GR32	4	42.3	82.3					58.9	59.2	113.9	0.99	2412.8

Accepted manuscript doi:
10.1680/jstbu.21.00116

Table 5 (a) Details of CFRFGs with different thicknesses

CFRFG Group	Specimen	Geometric details							$M_{u,FE}$ (kNm)	$M_{u,Calc}$ (kNm)	PNA, y_1 (mm)	$M_{u,FE}$ / $M_{u,Calc}$	As (mm^2)
		t_t mm	t_w mm	t_f mm	D_f mm	B_{Tf} mm	B_{Bf} mm	h_w (mm)					
G9	GR33	4	2.85	2.85	22.3	82.3	80	147	19.7	20.3	26.1	0.97	1420.2
	GR34	2.85	4	2.85	20	80			21.8	22.2	48.2	0.98	1354.0
	GR35	2.85	2.85	4	20	80			22.1	22.4	46.7	0.98	1277.0
G10	GR36	4	2.85	2.85	22.3	82.3	120	147	23.9	24.8	31.4	0.96	1534.2
	GR37	2.85	4	2.85	20	80			25.7	26.5	59.3	0.97	1468.1
	GR38	2.85	2.85	4	20	80			27.4	28.1	68.1	0.97	1437.0
G11	GR39	4	2.85	2.85	22.3	82.3	80	250	39.9	40.8	44.2	0.97	1713.3
	GR40	2.85	4	2.85	20	80			44.6	45.7	92.6	0.98	1765.5
	GR41	2.85	2.85	4	20	80			46.7	47.5	89.2	0.98	1570.0
|G12	GR42	4	2.85	2.85	22.3	82.3	120	250	45.7	46.9	56.0	0.97	1827.3
	GR43	2.85	4	2.85	20	80			49.6	50.7	106.3	0.97	1879.5
	GR44	2.85	2.85	4	20	80			52.3	52.9	116.7	0.98	1730.0
G13	GR45	4	2.85	2.85	42.3	82.3	80	127	21.8	23.3	38.8	0.93	1523.2
	GR46	2.85	4	2.85	40	80			22.7	23.9	58.3	0.95	1388.1
	GR47	2.85	2.85	4	40	80			23.3	24.4	57.4	0.95	1334.0
G14	GR48	4	2.85	2.85	42.3	82.3	120	127	25.9	26.8	45.3	0.97	1637.2
	GR49	2.85	4	2.85	40	80			26.6	27.2	67.8	0.97	1502.1
	GR50	2.85	2.85	4	40	80			28.8	29.3	74.3	0.98	1494.0
G15	GR51	4	2.85	2.85	42.3	82.3	80	250	44.4	46.8	60.5	0.95	1873.3
	GR52	2.85	4	2.85	40	80			51.0	53.6	105.6	0.95	1879.5
	GR53	2.85	2.85	4	40	80			54.4	55.6	99.3	0.98	1684.0

|G16	GR54	4	2.85	2.85	42.3	82.3	120	250	50.1	52.9	70.3	0.95	1987.3
	GR55	2.85	4	2.85	40	80			57.3	59.7	118.2	0.96	1993.5
	GR56	2.85	2.85	4	40	80			60.2	62.8	123.5	0.96	1844.0

Table 5 (b) Details of SRFGs with different thicknesses

SRFG Group	Specimen	Geometric details							$M_{u,FE}$ (kNm)	$M_{u,Calc}$ (kNm)	PNA, y_1 (mm)	$M_{u,FE}$ / $M_{u,Calc}$	As (mm^2)
		t_t mm	t_w mm	t_f mm	D_f mm	B_{Tf} mm	B_{Bf} mm	h_w (mm)					
G17	GR57	4	2.85	2.85	22.3	82.3	80	147	18.2	18.9	51.6	0.96	1420.2
	GR58	2.85	4	2.85	20	80			18.4	18.9	54.8	0.97	1354.1
	GR59	2.85	2.85	4	20	80			19.0	19.6	55.4	0.97	1277.0
G18	GR60	4	2.85	2.85	22.3	82.3	120	147	22.8	23.6	58.7	0.97	1534.2
	GR61	2.85	4	2.85	20	80			21.3	21.9	69.1	0.97	1468.1
	GR62	2.85	2.85	4	20	80			23.4	23.8	83.5	0.98	1437.0
G19	GR63	4	2.85	2.85	22.3	82.3	80	250	37.4	38.1	51.7	0.98	1713.3
	GR64	2.85	4	2.85	20	80			37.2	37.4	106.3	0.99	1765.5
	GR65	2.85	2.85	4	20	80			36.3	36.3	106.8	0.99	1570.0
G20	GR66	4	2.85	2.85	22.3	82.3	120	250	43.1	45.8	71.7	0.94	1827.3
	GR67	2.85	4	2.85	20	80			40.4	41.7	120.6	0.97	1879.5
	GR68	2.85	2.85	4	20	80			40.7	42.0	134.9	0.97	1730.0
G21	GR69	4	2.85	2.85	42.3	82.3	80	127	17.6	18.7	58.1	0.94	1523.2
	GR70	2.85	4	2.85	40	80			18.4	19.4	50.6	0.95	1388.1
	GR71	2.85	2.85	4	40	80			19.2	19.7	45.4	0.97	1334.0
G22	GR72	4	2.85	2.85	42.3	82.3	120	127	22.7	23.9	65.2	0.95	1637.2
	GR73	2.85	4	2.85	40	80			21.3	22.2	64.8	0.96	1502.1
	GR74	2.85	2.85	4	40	80			23.1	23.5	73.5	0.98	1494.0

Accepted manuscript doi:
10.1680/jstbu.21.00116

G23	GR75	4	2.85	2.85	42.3	82.3	80	250	40.6	42.3	43.7	0.96	1873.3
	GR76	2.85	4	2.85	40	80			41.3	41.9	112.1	0.98	1879.5
	GR77	2.85	2.85	4	40	80			40.2	40.6	106.8	0.99	1684.0
G24	GR78	4	2.85	2.85	42.3	82.3	120	250	46.8	48.8	63.7	0.96	1987.3
	GR79	2.85	4	2.85	40	80			44.9	45.9	126.3	0.98	1993.5
	GR80	2.85	2.85	4	40	80			45.2	46.0	134.9	0.98	1844.0

Figure captions

Fig. 1 Schematic of the concrete filled rectangular flange girder and cross-section (all dimensions are in mm)

Fig. 2 Stress-strain curve for materials used in CFRFGs including (a) the bilinear stress–strain curve adopted for the steel elements and (b) the assumed material model for the confined concrete

Fig. 3 Loading and boundary conditions in the FE model

Fig. 4 Validation of the FE model for (a) concrete filled rectangular flange girders (CFRFGs) and (b) steel rectangular flange girders (SRFGs)

Fig. 5 Distributions of strain and stress for (a) Case 1 where the PNA exists in the web of the steel section (i.e. $y_1 > D_f$) and (b) Case 2, where the PNA exists in the tubular flange section (i.e. $y_1 < D_f$)

Fig. 6 Ultimate moment versus deflection responses for (a) CFRFGs (b) SRFGs with different width-to-depth ratios (B_{Tf}/D_f)

Fig. 7 Ultimate moment versus deflection responses for (a) CFRFGs (b) SRFGs with difference web panel aspect ratios

Fig. 8 Ultimate moment versus deflection responses for (a) CFRFGs (b) SRFGs with difference web height

Fig. 9 Ultimate moment versus deflection responses for (a) CFRFGs (b) SRFGs with difference tensile flange width

Accepted manuscript doi:
10.1680/jstbu.21.00116

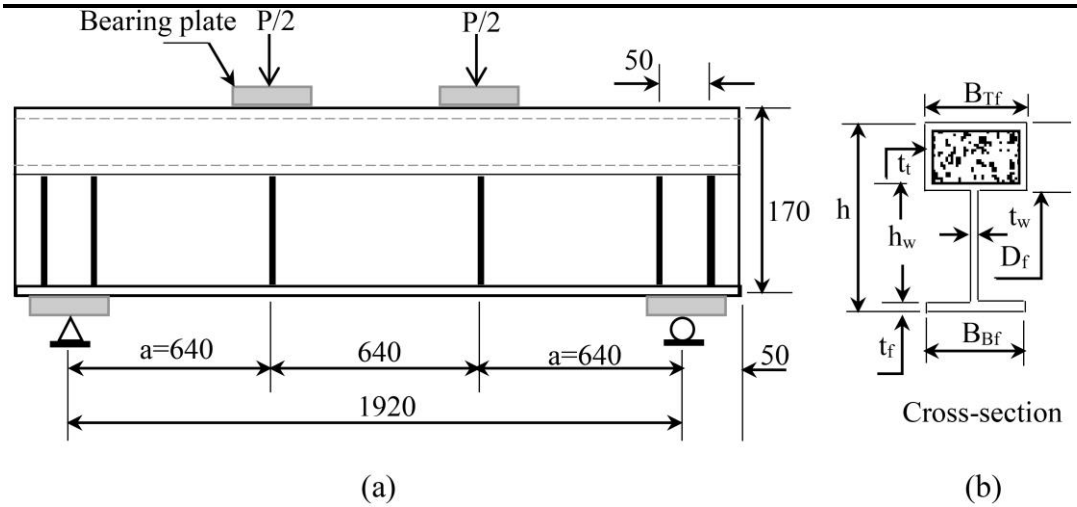

Fig. 1

Accepted manuscript doi:
10.1680/jstbu.21.00116

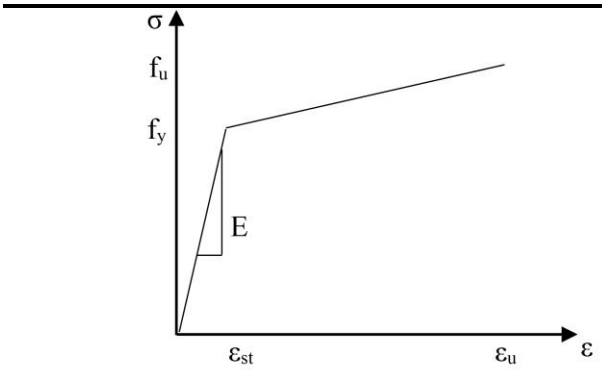

(a)

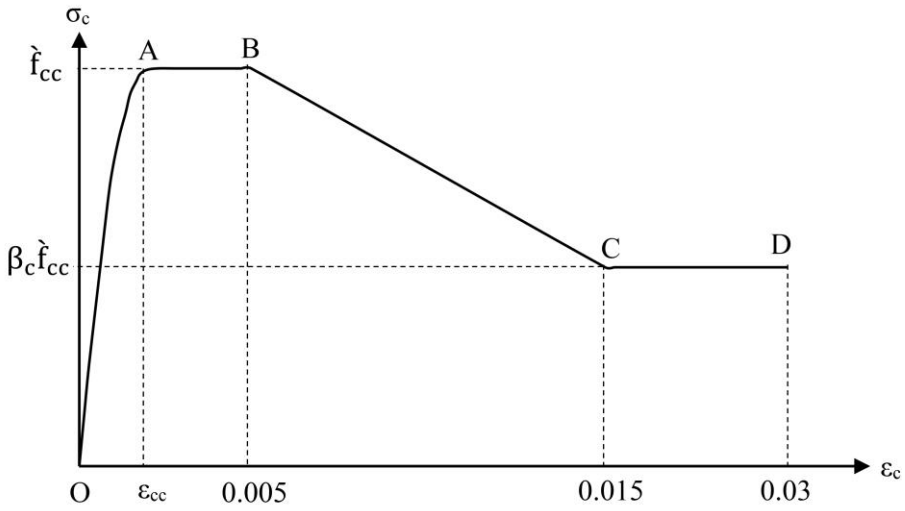

(b)

Fig. 2

Accepted manuscript doi:
10.1680/jstbu.21.00116

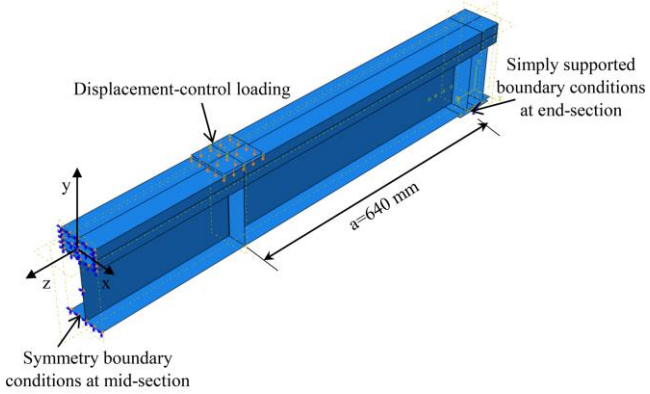

Fig. 3

Accepted manuscript doi:
10.1680/jstbu.21.00116

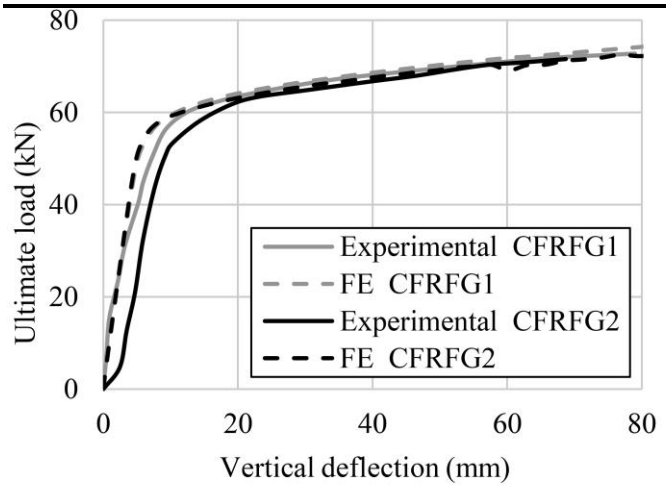

(a)

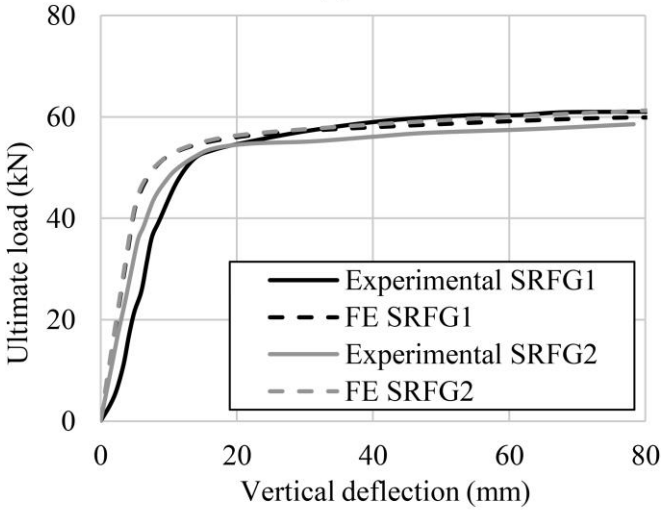

(b)

Fig. 4

Accepted manuscript doi:
10.1680/jstbu.21.00116

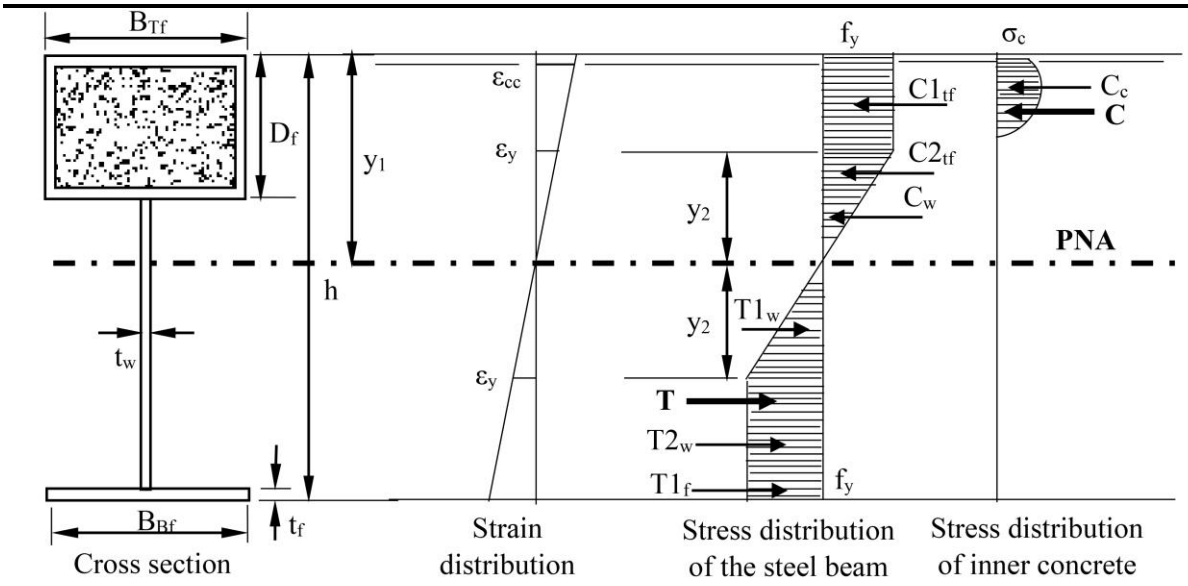

(a)

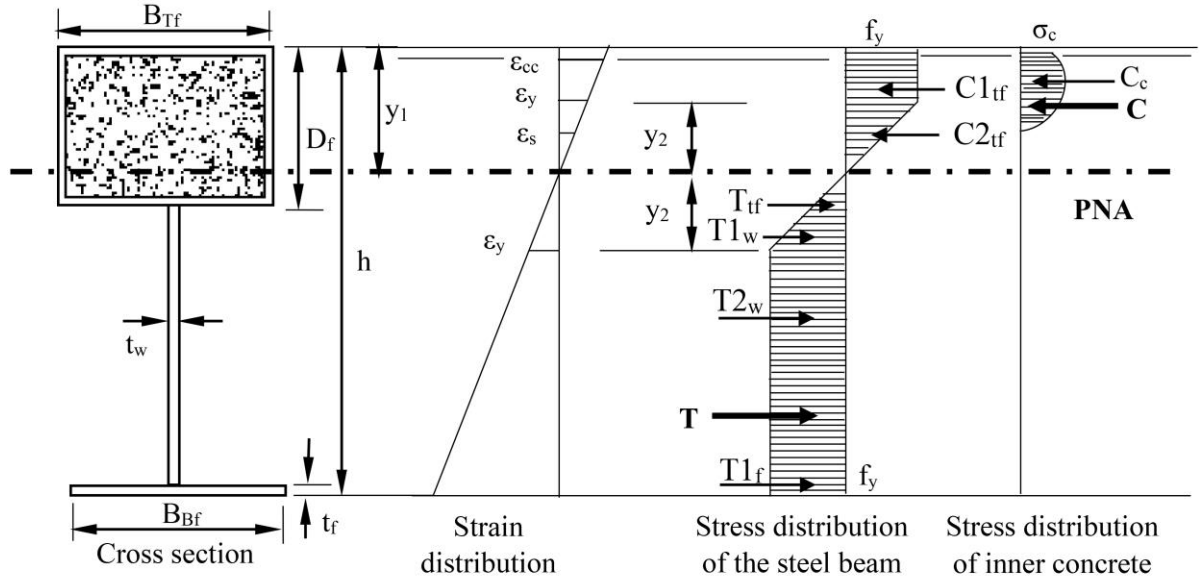

(b)

Fig. 5

Accepted manuscript doi:
10.1680/jstbu.21.00116

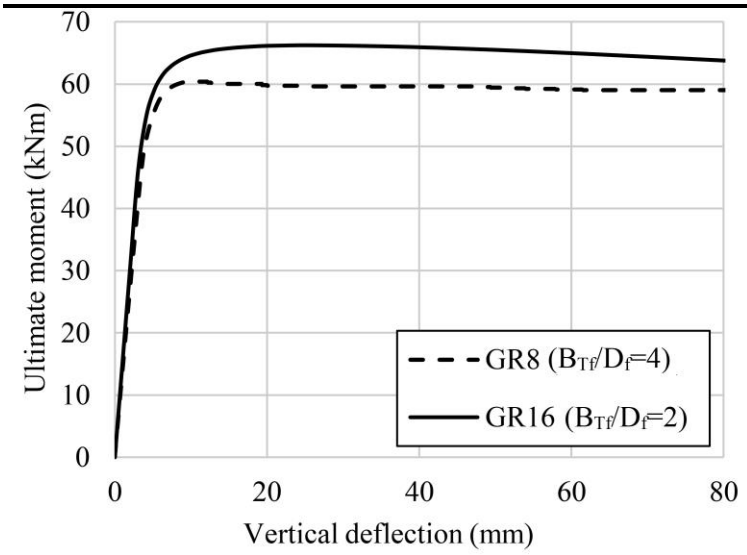

(a)

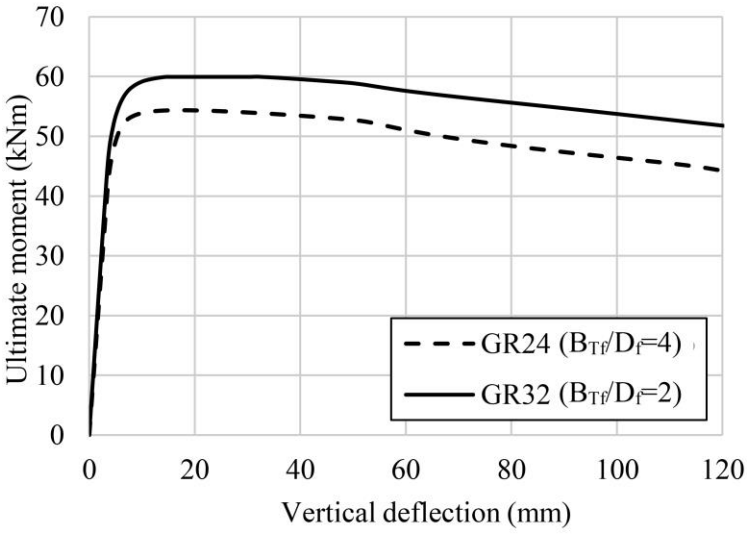

(b)

Fig. 6

Accepted manuscript doi:
10.1680/jstbu.21.00116

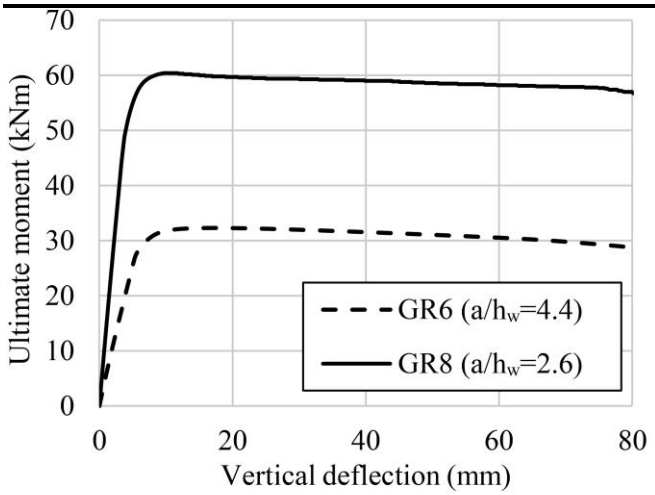

(a)

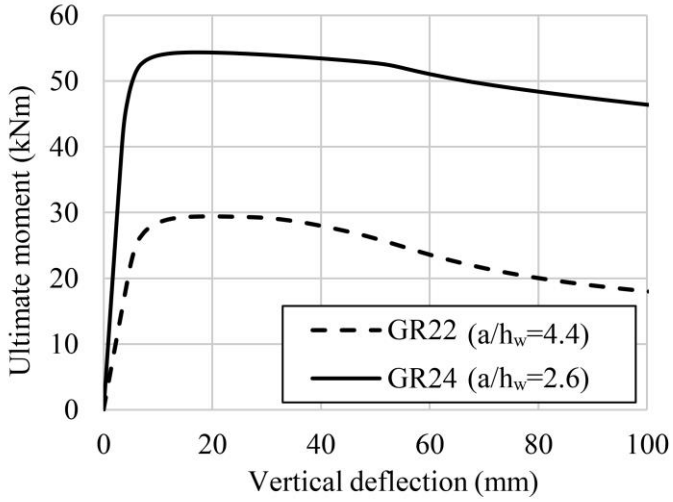

(b)

Fig. 7

Accepted manuscript doi:
10.1680/jstbu.21.00116

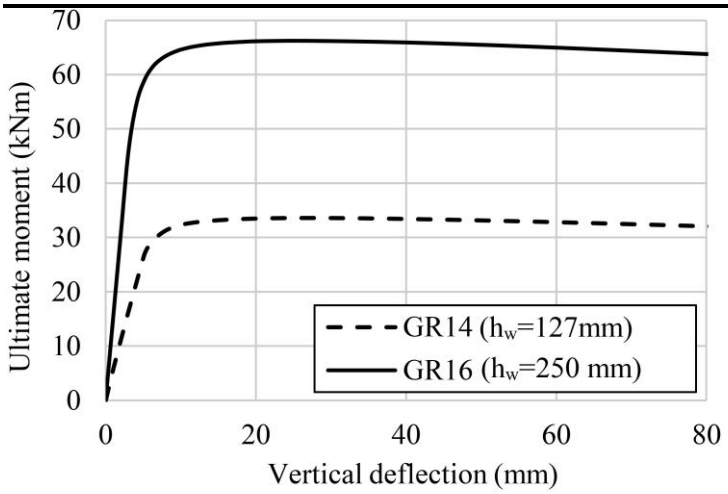

(a)

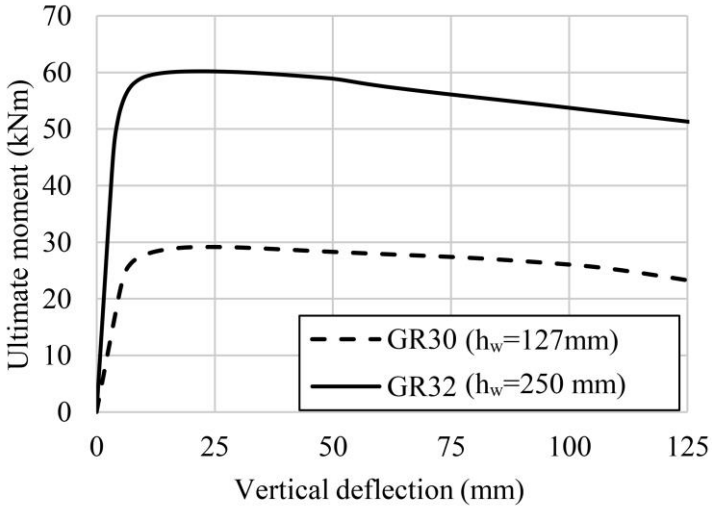

(b)

Fig. 8

Accepted manuscript doi:
10.1680/jstbu.21.00116

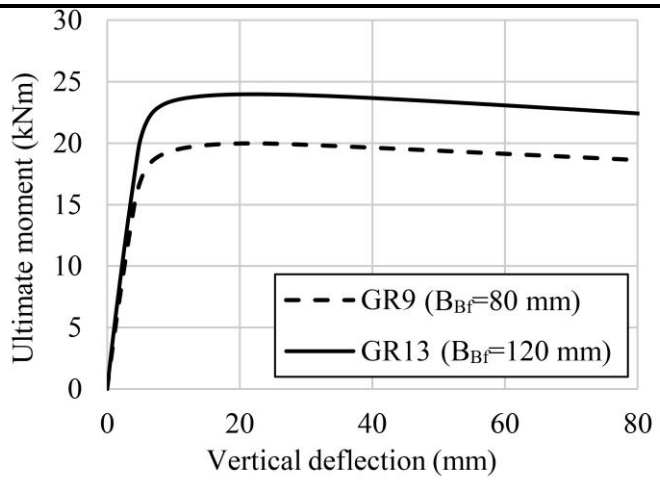

(a)

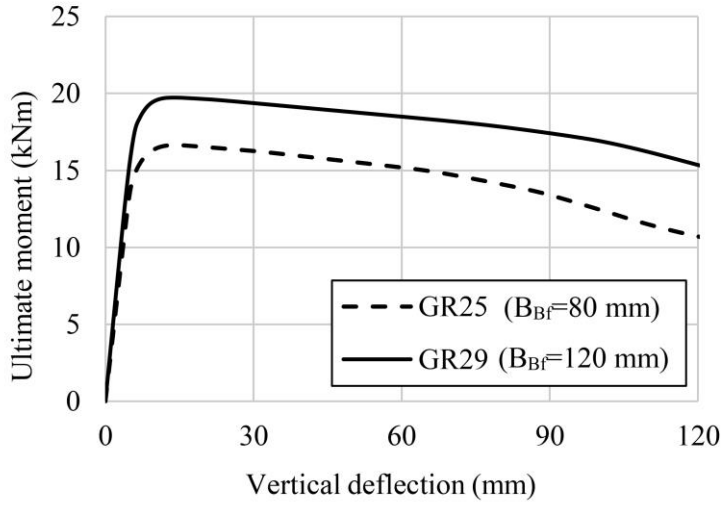

(b)

Fig. 9